# CrystEngComm

Accepted Manuscript






ROYAL SOCIETY OF CHEMISTRY

www.rsc.org/crystengcomm

# Calcium Oxalate Crystallization in the Presence of Amphiphilic Phosphoproteins

Yan Liu, Huiyuan Mao, Xifang Liu, Longjiao Qiao, Rong Guo*

College of Chemistry and Chemical Engineering, Yangzhou University, Yangzhou, 225002, P. R. China

To gain more insight into protein structure–function relationships that govern biomineralization is an exciting and challenging task. The influence of casein protein on the crystallization of calcium oxalate has been investigated in order to determine the roles of amphiphilicity and phosphate groups of proteins in the morphology and the phase control of the calcium oxalate crystals. The crystals obtained were characterized by scanning electron microscopy, Fourier-transform infrared spectroscopy, X-ray powder diffraction, and thermal gravimetric analyzer. The results show that, calcium oxalate monohydrate (COM) was obtained in the absence of proteins, while the obtained crystals were calcium oxalate dihydrate (COD) in the presence of casein. Casein can be assumed to take a key role during dumbbell shaped COD formation where it serves as an effective stabilization agent for COD and assembles nanorods into dumbbell COD. Compared to controls containing casein hydrolysate or bovine serum albumin (BSA), the stabilizing effect of casein arises from the electrostatic attraction between phosphate groups as well as carbonate groups (especially the former) and the calcium ions on the COD. The assembling effect of casein mainly comes from the hydrophobic interaction between casein molecules bound on COD nanorod surface. In addition, the presence of casein inhibits the crystallization process of calcium oxalate significantly. Our studies may contribute to the understanding of the specific role of amphiphilic phosphoprotein in the biomineralization process.

*To whom correspondence should be addressed. Tel：+86-514-87971802, Fax：+86-514-87311374, Email: guorong@yzu.edu.cn.

## Introduction

Biomineralization，a very common and important phenomenon in nature, has become an active area of research recently.[1-3] A key principle in the nature biomineralization is the involvement of biomolecules that modify or direct crystal growth and assembly.[4-10] It has been demonstrated by in vitro experiments that proteins can influence precipitated crystals, including the nucleation, polymorph selection, crystal growth, and crystal morphology. Inspired by nature, biomolecules are increasingly being used in nanotechnology to produce materials with ordered structures and desirable properties.[11-19] This will contribute to understanding biomineralization, with the benefits of not only uncovering the mechanism adopted by organisms but also applying them to the synthesis of hierarchical materials.[20-25]

Calcium oxalate (CaOx) is found in various shapes, phases, and properties in plants, and in pathological kidney or urinary stones.[26-29] The understanding of the crystal growth of calcium oxalate and its inhibition has always been a topic of interest in medicine, materials science, and industry.[30,31] Many studies have investigated how plants could control the formation of different calcium oxalate forms and how diseases like kidney stones could be avoided.[32-35] It is found that proteins modulating the mineralization of calcium crystals in a variety of organisms have an abundance of acidic amino acid residues.[36-40] Moreno et al. showed that the proteins from bean seed coat (Phaseolus vulgaris) were strong inhibitors of the nucleation of calcium oxalate monohydrate in vitro. Based on earlier studies, the author demonstrated that the proteins were acidic proteins rich in aspartic and glutamic. Unfortunately, the full sequence and the 3D structure of these proteins were necessary to identify the amino acid composition and the overall charge distribution.[41] Particularly, some earlier studies have shown that phosphorylated

proteins are engaged in biomineral formation. Osteopontin (OPN) is a prototype of such proteins, and contains a high content of phosphoserine, aspartate, and glutamate residues. OPN is a well-characterized CaOx crystal-modulating protein, and can inhibit COM formation while promote COD precipitation. It is found that phosphate groups in OPN play crucial roles in promoting COD over wide concentration ranges.[42-45]

These studies suggest that the amino acid composition and sequence as well as molecular structure are all crucial for the function of the proteins controlling crystallization of calcium oxalate. Due to the wide variety of sequence, size, amphiphilicity and charge of the protein, the mechanisms involved in the interaction of proteins with the inorganic phase have not yet been fully elucidated. The effect of proteins with well-defined amino acid sequences and molecular structures on CaOx crystallization is attracting much attention. No systematic investigations have been done so far on how the amphiphilicity and the phosphate groups of acid proteins affect the crystallization of biominerals CaOx cooperatively. One important source of acid phosphoproteins-casein can be thought of as amphiphilic block copolymers consisting of blocks with high levels of hydrophobic or hydrophilic amino acid residues, and the isoelectric point of casein is 4.5.[46] In this work, mineralization of CaOx has been investigated in the presence of casein. The influence of reaction time, temperature, pH and reagent concentration on the mediation of the phase transformation and morphology change of CaOx crystals in the presence of casein has been investigated systematically. The aim of the work is to understand how metastable phases COD are stabilized and how COD crystal with exquisite morphology formation takes place in the presence of amphiphilic phosphoprotein. These studies provide the first information about the roles of amphiphilicity,

phosphate and carboxylate groups of proteins in modulating the crystallization of CaOx.

**Experimental Section**

**Materials.** Casein (isoelectric point (pI) = 4.5 and average molecular weight (MW) = 2.1 kDa), bovine serum albumin (BSA) and casein hydrolysate were purchased from Sigma. Analytical grade sodium oxalate and calcium chloride were purchased from Shanghai Chemical Reagent Company and used as received without further purification. Distilled water was used as the solvent.

**Experimental Procedures.** Stock solution of 1.0 M calcium chloride and 200 mM sodium oxalate were first prepared as stock solutions. In a typical procedure, 0.05 ml of 1.0 M $CaCl_2$ aqueous solution was added to 49.95 mL of 4.0 g/L soluble casein aqueous solution, and the pH of the solution was adjusted to a desired pH (e.g., pH 6.5) by using HCl or NaOH solution. This gave the $CaCl_2$ concentration of 1.0 mM in the casein/ $CaCl_2$ solution, and the solution was stirred for 30 min (1500 rpm). Then, 50 mL of sodium oxalate solution (1.0 mM) was added rapidly into the above solution to start the mineralization process of $CaC_2O_4$ under stirring. Upon the addition of sodium oxalate solution, the system pH varies from pH 6.5 to 6.9. After stirring for 24 h (800 rpm), the obtained precipitate was centrifuged and rinsed at least three times with distilled water and ethanol and dried at room temperature. During the experimental process, all solutions were placed in a thermostated vessel to maintain the reaction temperature.

**Characterization.** X-ray powder diffraction (XRD) patterns were recorded using a Bruker D8 Advanced XRD diffractometer with Cu KR radiation at a scanning rate of 0.04 degree$\cdot s^{-1}$. Scanning electron microscope (SEM) images were taken with a JEOL JSM-6700FXIB, fitted with a field emission source, and working at 20 kV. All

samples were mounted on copper stubs and sputter coated with gold prior to examination. Infrared spectroscopic analysis was performed in transmission mode (FT-IR) using a Nicolet Aexus 470, with scanning from 4000 to 500 $cm^{-1}$ by using KBr pellets. The transmission electron microscope (TEM) measurements were carried out using a TEM instrument (Philips, Tecnai 12). The conductivities of the samples were measured with a DDS-11A digital conductivity meter (Shanghai Tianda Precision Instrument Co. Ltd.) calibrated using aqueous KCl solutions.

**Results and Discussion**

The crystallization of CaOx results in a nearly closed dumbbell-shaped particle of about 4.5 μm when casein is used as an additive (Fig. 1a). The magnified SEM image reveals that the obtained CaOx dumbbell consists of a large quantity of nanorods with diameter of about 50 nm and length up to several microns (Fig. 1b). The crystalline phases of CaOx precipitates were verified using XRD and FTIR analysis (Fig. 2a and b). Fig. 2a shows the XRD pattern of CaOx precipitates, revealing reflection peaks for COD crystals.[26] Notably, the XRD pattern of CaOx sample shows the (512) reflection is considerably intensified compared with the standard diffraction intensities of COD. This indicates the adsorption of the protein on the COD (512) plane is favored at the experimental condition, leading to a preferential alignment of the (512) plane of COD. XRD patterns were further analyzed using the Scherrer formula $D_{hkl} = k\lambda/\beta\cos\theta$,[47,48] where $D_{hkl}$ is the coherence length of the crystalline domain perpendicular to the respective *hkl* plane, $k$ is a constant of 0.89, $\lambda$ is the X-ray wavelength (Cu Kα = 0.154 nm), $\beta$ is the background-corrected line broadening in degrees, (π/180) is a correction factor to calculate $\beta$ in radians, and $\theta$ is the scattering angle. The coherence lengths (crystallite sizes, $D_{hkl}$) calculated via the Scherrer equation are shown in Table 1. The $D_{hkl}$ values for the sample at (200), (211) and (411) reflection are 36.2 nm, 29.3 nm

and 29.5 nm, respectively. Evidently, the $D_{hkl}$ values is close to the width of ca. 50 nm of the nanorods obtained from SEM, but is much shorter than the length of the nanorods obtained from SEM. This suggests that the nanorods are composed of primary nanoparticle, and these nanorods further assembly into the dumbbell-shaped superstructure.

The phase of the product was also confirmed by the FTIR spectrum (Fig. 2b). The presence of the antisymmetric carbonyl stretching band from oxalate at 1645 $cm^{-1}$ and the symmetric carbonyl stretching band at 1323 $cm^{-1}$ can be assigned as the characteristic peaks for COD.[28] Two characteristic transition bands located at 916 and 613 $cm^{-1}$ in the fingerprint region support this conclusion. It was found that the morphologies and polymorphs of the samples were not changed after more than five months (Figs. S1-2, Supporting Information). As a control, the SEM and XRD results indicate that the crystals of hexagonal COM and a few flowerlike COM agglomerates are formed during crystallization of calcium oxalate in the absence of protein (Fig. 3). Thus, casein is able to stabilize the metastable phases of calcium oxalate, COD, avoiding the conversion to the thermodynamically stable phase, COM.

Recently, it was suggested that incorporation of (macro) molecules into a growing crystal can significantly increase the long-term stability of metastable phases. Casein with an isoelectric point of about 4.5 is negatively charged at neutral pH, and has several phosphoserine residues in addition to a highly content of acid amino acid residues (such as glutamic acid and aspartic acid residues). Thus, casein has the ability to bind calcium ions via both phosphate groups of phosphoserine, and carboxylate groups of acid amino acid residues, which contributes to the formation of COD. The thermogravimetraic analysis (TGA) results confirm that casein molecules remain attached in the separated samples. Compared with the typical three stages of

weight loss for COD without the existence of any additive, CaOx precipitates mineralized in the presence of casein show the weight loss of 15 wt % at around 250 − 450 °C due to the decomposition of protein (Fig. 2c). The characterized dehydration process of 19.43% occurs at 180 °C, which is very close to the theoretical value of 20.56% for calcium oxalate dihydrate. The results indicate that the presence of casein has a stabilizing effect on the unstable COD phase, blocking its transition to the COM phase.

To determine which interaction (binding between calcium ions and phosphate groups or carboxylate groups) plays a crucial role in the stabilization of COD, a controlled experiment with the additive BSA was performed, and the products are mainly elongated hexagonal COM (Fig. 4). Compared with casein, BSA contains higher content of aspartate and glutamate residues, but no phosphoserine residues. The results confirm that the stabilization of COD could only be achieved by strong interaction of phosphate groups of casein and the calcium ions on the COD surface. Notably, compared with the content of acid amino acid residues (40 %), the content of the phosphate group (2.5 %) is very low in casein. However, the phosphate group in casein still plays a crucial role in the formation and stabilization of COD.

To further demonstrate the roles of casein in CaOx crystallization, we conducted the effects of the casein concentration, the ion concentration, pH and temperature on the crystallization of CaOx in the presence of casein.

The variation of casein concentration can effectively modulate the morphologies of CaOx. When the casein concentration is decreased to 0.2 g $L^{-1}$, tetragonal bipyramidal COD are mainly obtained (Fig. 5a). With the casein concentration increasing to 0.5 g $L^{-1}$, a small amount of nearly closed dumbbell-shaped particles

and a large proportion of twined spherical particles are obtained (Fig. 5b). With the further increase of casein concentration to 1.0 g $L^{-1}$, the twined spheres and the nearly closed dumbbell-shaped particles are still obtained, but the proportion of the latter increases (Fig. 5c). As the casein concentration continuously increases to 6 g $L^{-1}$ (Fig. 5d), the dumbbell shaped crystals with about 10.0 μm in length and 3.0 μm in width are obtained. As shown in the enlarged SEM image of the opened CaOx dumbbell (inset of Fig. 5d), the CaOx dumbbell is also stacked of nanorods. All peaks of the XRD patterns of the obtained CaOx samples are exactly matched with the standard XRD data of COD (Fig. S3A), indicating the formation of completely COD in the presence of casein with various concentrations. Interestingly, the XRD pattern of CaOx sample obtained in the presence of 6 g $L^{-1}$ casein shows the (400) reflection is considerably intensified compared with the standard diffraction intensities of COD. This indicates the adsorption of the protein on the COD (400) planes is favored with increasing casein concentration, leading to a preferential alignment of the (400) plane of COD. As mentioned above, CaOx sample obtained in the presence of 2 g/L casein shows the considerably intensified (512) reflection compared with the standard diffraction intensities of COD. Thus, casein of different concentration has different effect on crystal face. As is well known, the binding behavior of macromolecules to crystal faces is very complex. The detailed reason for the difference remains unclear at present.

To examine the effect of the calcium concentration on the crystallization, the crystallization experiment was repeated at a protein concentration of 4.0 g $L^{-1}$ but at

lower and higher $CaCl_2$ concentrations. At a lower $CaCl_2$ concentration of 0.8 mM, the product is dumbbell shaped crystals (Fig. 6a). Due to the small amount of CaOx sample obtained at low ion concentration, XRD measurement could not be conducted. However, the characterized peak at 1645 and 1323 $cm^{-1}$ in the FTIR spectrum confirmed the formation of COD. These dumbbell COD crystals are similar to those obtained at a $CaCl_2$ concentration of 1.0 mM but at a higher protein concentration of 6 g $L^{-1}$ (Fig. 5d), although the present dumbbell shaped crystals are much smaller (less than 2.0 μm in length and 0.4 μm in width). On the other hand, at a higher $CaCl_2$ concentration of 2.0 mM, twined spherical particles are obtained (Fig. 6b). XRD results confirmed the formation of COD (Fig. S3D). These results suggest that decreasing the $CaCl_2$ concentration at a fixed protein concentration has a similar effect as increasing the protein concentration at a fixed $CaCl_2$ concentration.

Generally, temperature is believed to have a great impact on the crystal forms of the final products. We have carried out analogous experiments at different temperatures. Fig. 7a shows that twined spherical particles are mainly produced at 10 ± 1 °C. With the reaction temperature increasing to 37 ± 1°C, dumbbell shaped CaOx with loose structure are observed (Fig. 7b). The CaOx samples obtained at lower and higher temperatures both can be indexed as COD (Fig. S3B, Supporting Information), indicating the temperature has no effect on the polymorph CaOx in the presence of casein. Here, casein has been classified as an "intrinsically unstructured/disordered" protein due to the presence of a high content of proline residues, so casein has no obvious secondary structure. The increase of temperature from 10 to 37 °C will not change the protein structure obviously. As is well known, the movement speed of both polymer and nanoparticles increases with temperature. The increase of temperature results in a faster speed of protein and mineral nanocrystal motion. Thus, casein may

preferentially interact with CaOx nanocrystals, and hence the gradual morphological transition of COD crystals from twined spherical particles to dumbbell shaped particles.

The variation of pH also can change the morphology and phase of the produced CaOx crystal. Experiments were conducted under the standard conditions at other two typical starting pH, including pH 3.5 and 10.5. At pH 10.5, where the pH is above the pI value of casein (pI=4.5), dumbbell shaped CaOx is obtained (Fig. 8a). The CaOx sample prepared is COD as indexed in both XRD (Fig. S3C) and FT-IR results (Fig. S4). However, elongated hexagonal flake COM is obtained at pH 3.5 where pH is below the pI of casein (Fig. 8b). FTIR results show that CaOx sample prepared at pH 3.5 is COM (Fig. S4). It can be seen that lower pH is not favorable for the formation of COD. At pH below pI of casein, the electrostatic attraction between $Ca^{2+}$ and the negatively charged groups is reduced much due to the almost protonated acid groups in casein. Therefore, the strong binding of casein on CaOx surface is inhibited, and COD can not be obtained in this case. At higher starting pH, acid groups in casein are deprotonated, resulting in strong interaction between casein and the growing CaOx. Consequently, the crystallization of stable-phase COM is inhibited and dumbbell-shaped COD is formed. As a control, the CaOx crystallization without proteins at different pH (pH 3.5 and 10.5) were conducted. Similar to pH 6.8, CaOx samples formed at pH 3.5 display hexagonal COM and flowerlike COM aggregates (Fig. S5). Differently, CaOx samples formed at 10.5 show mainly tabular COT and hexagonal COM, which may be caused by the high supersaturation at high solution pH (Fig. S5). Obviously, pH has much different effects on the CaOx crystallization with and without protein. This confirms that the effect of pH on the CaOx crystallization in the presence of casein is due to the different interaction between

protein and CaOx nanocrystal at different starting pH. Notably, different from our results here, COT was formed at acid system in some earlier studies.[49] The reason for the different results at acid condition is a result of the reaction environment. In the earlier study, pH 1.2, 12 °C and molar ratio of oxalic acid to calcium chloride being 0.75 were used, and the dropwise addition of oxalic acid into calcium chloride solution was performed in the experiment. Here, pH 3.5, 25 °C and molar ratio of oxalic acid to calcium chloride being 1.0 were used, and the rapid addition of oxalic acid into calcium chloride solution was performed.

The crystal properties of calcium oxalate obtained in the presence of casein together with the experimental conditions have been summarized in Table 2. The information listed in Table 2 indicates that the lower starting pH leads to the formation of COM, while the higher starting pH favors the formation of COD in the presence of casein irrespective of the other experimental conditions. With increasing [casein]/[$Ca^{2+}$] ratio, the interaction between protein and CaOx becomes stronger, leading to a gradual morphological transition of COD crystals from bipyramidal shaped crystals to twined spherical particles, and subsequently to nearly closed dumbbell shaped particles and then to dumbbell shaped particles. Similarly, temperature changing from 10 to 35°C leads to morphological transition of COD crystals from nearly closed dumbbell shaped particles to dumbbell shaped particles.

To obtain more information about the roles of casein in the formation of dumbbell-shaped particles, the phase and morphological development of CaOx at different crystallization times was examined. The representative TEM, SEM images and FTIR patterns of the products obtained at the early stages of the superstructure formation are presented in Fig. 9 and Fig. S6.

FTIR results showed that the polymorphs of products obtained after 3 h of reaction are all COD phase (Fig. S6). Before 3 h, FTIR analysis could be hardly performed because of the small amount of the sample. The time-resolved FTIR patterns indicated that the growth of aggregates did not go through any polymorph transformation.

An examination of the intermediate products collected after 30 min show that there are a very small amount of nanorods with diameters of about 50 nm (Fig. 9a). The above XRD results indicate that these nanorods are already composed of primary particles. However, primary particles cannot be directly observed though TEM images, presumably because these primary particles are not stable and are easy to assemble into nanorods with the help of proteins. With an increase in the reaction time to 5 h, nanorod bundles were observed (Fig. 9b). During the process, the length of the nanorods in the bundles increases with the diameter remaining almost constant. With an increase in the reaction time, these nanorod bundles branched at their ends and dumbbell-like nanorod bundles were observed (Fig. 9c). By further prolonging the reaction time to 12 h, these nanorod bundles further branched at their ends and developed into nearly closed dumbbell-like superstructures (Fig. 9d). These intermediates suggest that the final stage of almost closed dumbbells results from a complex growth mechanism, which was called the "rod-to-dumbbell-to-sphere" transformation mechanism.[50] In this mechanism, rodlike particles are formed first, and stack into rodlike bundles. Then these rodlike bundles can grow at their ends resulting in dumbbell-like bundles, where crystal splitting is the main reason for the initial branching from rods to dumbbells.[51] These dumbbells grow further into nearly closed dumbbells when the reaction is performed for a long enough time. Crystal splitting is generally associated with fast crystal growth and is caused by internal crystal strain (defects) and high supersaturation of the surrounding medium.[42] Even though the

"rod-to-dumbbell-to-sphere" transition seems to be a general crystal growth phenomenon and was observed for several carbonate systems ($CaCO_3$, $BaCO_3$, $MnCO_3$, and $CdCO_3$) as well as a fluoroapatite system ($Ca_5(PO_4)_3OH$), it was first been observed in the mineralization of calcium crystals under the control of protein. The structures and the crystalline evolution process of the superstructures suggest that the formation mechanism is a typical nonclassical pathway of crystallization, including the self-assembly of the primary particles with the help of the additive. The mode of self-assembly of nanoscale building blocks under control of casein agrees well with the growth model proposed by Colfen et al.[52]

Just as discussed above, the contributions of phosphate groups in caseins are important determinants of the stabilization of COD. In addition to the role of stabilizing COD, the amphiphilic phosphoprotein significantly induce morphological changes in growing COD crystals and aggregates. The amphiphilic caseins interact with crystal surfaces via phosphate and carboxylic groups in the hydrophilic chain, leaving the hydrophobic chains exposed to inhibit crystal growth into bipyramidal COD. This results in the formation of rod like particles. The hydrophobic interaction between the bound casein molecules may be one of the main driving forces for the rod like particle assembly. Then, the nanorod bundles grow at their ends, resulting in dumbbell shaped COD.

To determine whether the amphiphilicity of casein plays a crucial role in the formation of the dumbbell-shaped COD, we used casein hydrolysate as a control. The casein hydrolysate is mixtures of small peptides, and some of them bear phosphate groups. In the case of casein hydrolysate, the products are mainly elongated bipyramidal COD (Fig. 10). The results indicate that the small peptides can stabilize COD phase, but cannot lead to the formation of dumbbell shaped crystals. Thus, the

amphiphilicity of protein plays a deciding role in assembling nanorods into dumbbell COD.

The inhibition effect of caseins was also estimated by comparing the crystallization kinetics in their presence with a blank crystallization in the absence of any additives. The crystallization kinetics was studied by conductivity measurement. In the process of crystal growth, the total concentration of the conductive ions decreases due to the precipitation of CaOx crystals from the supersaturated solution. This results in diminished conductive capacity and declined conductivity. Therefore, the dynamic crystallization process of CaOx crystals can be monitored through the system conductivity change over time. The time between the generation of a supersaturated state and the first observed change in conductivity is defined as the induction period ($t_{ind}$). The effect of protein on the rate of precipitation of calcium oxalate can be quantified as the ratio of the initial slope of the curve of the pure solution at pH 6.9 and 25 °C ($k_0$) to the initial slope of the curves of solution with protein at different experimental conditions ($k_i$). Conductivity statistics recorded from the moment $CaCl_2$ and $Na_2C_2O_4$ mixed in aqueous solution without and with casein under stirring were shown in Fig. 11. As shown, the conductivity of the system with protein is higher than that without protein from the beginning, which is caused by the presence of negatively charged protein at neutral pH. It can be seen from Fig. 11, the conductivity of the system with no protein showed sharp dropping immediately and reached its precipitate dissolution equilibrium in only 20 min. Whereas, in the system with protein, the conductivity remained constant for about 15 min once $Ca^{2+}$ and $C_2O_4^{2-}$

solutions were mixed, and then decreased gradually and reached the precipitate dissolution equilibrium until 15 h. Thus, the rate of CaOx precipitation in the presence of protein was reduced drastically.

Many earlier studies found that carboxylate-containing macromolecules may exhibit an inhibitory effect on crystallization kinetics of CaOx due to the adsorption of macromolecules on the crystal surfaces.[18,26,30] Casein contains about 34% acid amino acid residues (such as glutamic acid and aspartic acid residues), so casein has the potential to adsorb on crystal surfaces because of the ionic attractive interactions between the carboxylate groups and the positive sites ($Ca^{2+}$) at the solution interface. Recently, it was shown that phosphorylation of OPN peptides increased their potency to inhibit COM crystallization.[7,13,18] Accumulating evidence suggests that phosphate groups provide a strong negative charge that electrostatically forces the molecule closer to crystal faces but that carboxylates, perhaps for stereochemical reasons, are capable of more specific interactions with cations.[7,31] In addition to the high content of glutamic acid and aspartic acid residues, casein has several phosphoserine residues. And more importantly, these several phosphoserine residues are adjacent to the glutamic acid residues. Therefore, the cooperation of phosphate and carboxylate groups leads to the efficient adsorption of casein on crystal surfaces, and hence a significant inhibition of calcium oxalate crystallization.

The inhibition results in the presence of casein together with the experimental conditions are summarized in Table 3. As shown, the inhibition results vary much according to the different experimental conditions. An increasing [casein]/[$Ca^{2+}$] ratio

increases induction time and $k_0/k_i$ drastically. With increasing [casein]/[$Ca^{2+}$] ratio, the interaction between protein and CaOx becomes stronger, leading to a drastically increased inhibition efficiency of protein.

The induction time increases from 6 s to 45 min, and $k_0/k_i$ increase from 10.3 to 352.0 when the temperature increases from 10 to 37 °C. This indicates that the inhibition efficiency of protein increases drastically with the increase of temperature. The rate of CaOx precipitation decreases since the supersaturation decreases with the increase of temperature. Furthermore, casein may preferentially interact with CaOx nanocrystals due to a faster speed of protein and mineral nanocrystal motion with the increase of temperature. Thus, the above two factors result in a drastically increased inhibition efficiency of protein, and hence an increased induction time and $k_0/k_i$ with increasing temperature.

Compared with the case at pH 6.9, both the lower and higher starting pH decrease induction time and $k_0/k_i$ drastically in the presence of casein irrespective of the other experimental conditions. Oxalic acid is a week acid, and the loss of the second proton, which yields the oxalate ion has an equilibrium constant of $5.25\times10^{-5}$ ($pK_a$ = 4.28). Thus, the oxalate ion concentraiton is high, resulting in a high supersaturation at high pH. Although the interaction between casein and the growing CaOx is stronger, the decreased induction time and $k_0/k_i$ may be caused by the high supersaturation at starting pH 10.5. Differently, the supersaturation is low at starting pH 3.5, but the binding of casein on CaOx surface is inhibited effectively due to the almost protonated carboxylate groups in casein. Maybe the latter factor plays a more crucial

role, which results in a sharp decline in inhibition efficiency of protein at starting pH 3.5.

## Conclusions

A key principle in the nature biomineralization is the involvement of proteins that manipulate and control the nucleation, orientation, and morphology of minerals. In the present work, we made use of an amphiphilic phosphoprotein, casein, to mediate the nucleation and growth of calcium oxalate. By regulating the synthesis condition such as temperature, the pH of the solution, the reaction time, and the concentration of casein, we can control the phase transformation and morphology change of CaOx crystals. Comparing the CaOx crystallization in the presence of BSA and casein hydrolysate, it was found that the phosphate groups of casein play a deciding role in the stabilization of the resulting COD crystals, and the amphiphilicity of the proteins assembles nanorods into dumbbell COD. Thus, both the amphiphilicity and the phosphate groups of protein are key factors in the ability of amphiphilic phosphoproteins to regulate biomineralization processes. The use of amphiphilic phosphoprotein in CaOx crystallization offers new insights into controlling the polymorphs and morphologies under easily attainable reaction conditions. Our studies also shed light on the mechanistic interpretation of biomimetic mineralization induced by proteins.

## Acknowledgments

This work was supported by the National Nature Science Foundations of China (21073156), PAPD and RFDP (20113250110007).

## References

1 J. J. De Yoreo and P. M. Dove, *Science*, **2004**, 306, 1301–1312.

2 A. Thomas, E. Rosseeva, O. Hochrein and R. Kniep, *Chem. Eur. J.*, **2012**, 18, 4000–4009.

3 X. H. Guo and S. H. Yu, *Crystal Growth & Design*, **2007**, 7, 354–359.

4 A. George and A. Veis, *Chem. Rev.*, **2008**, 108, 4670–4693.

5 G. K. Hunter, J. OuYoung, B. Grohe, M. Karttunen and H. A. Goldberg, *Langmuir,* **2010**, 26, 18639–18646.

6 M. Sarikaya, C. Tamerler, A. K. Jen, K. Schulten and F. Baneyx, *Nat. Mater.,* **2003**, 2, 577–585.

7 B. Grohe, J. OuYoung, D. A. Ionescu, G. Lajoie, K. A. Rogers, M. Karttunen, H. A. Goldberg and G. K. Hunter, *J. Am. Chem. Soc*., **2007**, 129, 14946–14951.

8 G. Falini, S. Albeck, S. Weiner and L. Addadi, *Science*, **1996**, 271, 67–69.

9 A. N. Kofina, K. D. Demadis and P. G. Koutsoukos, *Crystal Growth & Design,* **2007**, 7, 2705–2712.

10 M. F. Butler, N. Glaser, A. C. Weaver, M. Kirkland and M. Heppenstall-Butler, *Crystal Growth & Design,* **2006**, 6, 781–794.

11 S. Kirboga and M. Öner *CrystEngComm*, **2013**, 15, 3678-3686.

12 T. Jung, X. Sheng, C. K. Choi, W. S. Kim, J. A. Wesson and M. D. Ward, *Langmuir,* **2004**, 20, 8587–8596.

13 L. J. Wang, X. Y. Guan, R. K. Tang, J. R. Hoyer, A. Wierzbicki, J. J. De Yoreo and G. H. Nancollas, *J. Phys. Chem. B,* **2008**, 112, 9151–9157.

14 L. N. Hassani, F. Hindré, T. Beuvier, B. Calvignac, N. Lautram, A. Gibaudb and F. Boury, *J. Mater. Chem. B,* **2013**, 1, 4011-4019.

15 Y. Liu, Y. J. Cui, R. Guo, *Langmuir,* **2012**, 28, 6097–6105.

16 E. Akyol and M. Öner, *J. Cryst. Growth,* **2007**, 307, 137–144.

17 X. Sheng, M. D. Ward and J. A. Wesson, *J. Am. Chem. Soc.,* **2003**, 125, 2854–2855.

18 B. Grohe, A. Taller, P. L. Vincent, L. D.; K. A. Rogers, A. Heiss, E. S. Sørensen, S. Mittler, H. A. Goldberg and G. K. Hunter, *Langmuir,* **2009**, 25, 11635–11646.

19 J. D. Hartgerink, E. Beniash and S. I. Stupp, *Science,* **2001**, 294, 1684 –1688.

20 J. Aizenberg, D. A. Muller, J. L. Grazul and D. R. Hamann, *Science,* **2003**, 299, 1205–1208.

21 M. Sarikaya, C. Tamerler, A. K. Jen, K. Schulten and F. Baneyx, *Nat. Mater.,* **2003**, 2, 577–585.

22 S. Y. Lee, E. Royston, J. N. Culver and M. T. Harris, *Nanotechnology,* **2005**, 16, S435–S441.

23 L. P. Zhou, J. F. Ye, G. S. Hong and L. M. Qi, *Soft Matter,* **2011**, 7, 9624-9627.

24 X.Q. Li and H. C. Zeng, *Advanced Materials,* **2012**, 24, 6277-6282.

25 S. H. Yu, H. Cölfen, A. W. Xu and W. F. Dong, *Crystal Growth & Design,* **2004**, 4, 33–37.

26 B. Akın, M. Öner, Y. Bayram and K. D. Demadis, *Crystal Growth & Design,* **2008**, 8, 1997–2005.

27 S. Kırboğa and M. Öner, *Crystal Growth & Design,* **2009**, 9, 2159–2167.

28 J. M. Ouyang and S. P. Deng, *Dalton Trans.,* **2003**, 14, 2846–2851.

29 V. R. Franceschi and H. T. Horner, Calcium oxalate crystals in plants. *Bot. Rev.,* **1980**, 46,

361–427.

30 V. Fischer, K. Landfester and R. M. Espí, *Crystal Growth & Design,* 2011, 11, 1880–1890.

31 A. Taller, B. Grohe, K. A. Rogers, H. A. Goldberg and G. K. Hunter, *Biophysical Journal,* **2007**, 93, 1768–1777.

32 M. A. Webb, *Plant Cell,* **1999**, 11, 751–761.

33 A. M. Cody and H. T. Horner, *Scanning Electron Microscopy III:* **1984**, 1451–1460.

34 H. Shiraga, W. Min, W. J. VanDusen, M. D. Clayman, D. Miner, C. H. Terrell, J. R. Sherbotie, J. W. Foreman, C. Przysiecki and E. G. Neilson, *Proc. Natl. Acad. Sci. USA,* **1992,** 89, 426–430.

35 S. R. Qiu, A. Wierzbicki, C. A. Orme, A. M. Cody, J. R. Hoyer, G. H. Nancollas, S. Zepeda and J. J. De Yoreo, *Proc. Natl. Acad. Sci. USA,* **2004**, 101, 1811–1815.

36 A. M. Mazen, D. Zhang and V. R. Franceschi, *New Phytol.,* **2004**, 161, 435–448.

37 N. Bouropoulos, S. Weiner and L. Addadi, *Chem. Eur. J.,* **2001**, 7, 1881–1888.

38 T. S. Jung, W. S. Kim and C. K. Choi, *J. Cryst. Growth,* **2005**, 279, 154–162.

39 J. F. Liu, H. D. Jiang and X. Y. Liu, *J. Phys. Chem. B,* **2006**, 110, 9085–9089.

40 L. Addadi and S. Weiner, *Proc. Natl. Acad. Sci. USA,* **1985**, 82, 4110–4114.

41D. Jáuregui-Zúñiga, J. P. Reyes-Grajeda and A. Moreno, *Plant Science,* 2005, 168, 1163-1169.

42 L. A. Thurgood, A. F. Cook, E. S. Sørensen and R. L. Ryal, *Urol Res,* **2010**, 38, 357–376.

43 L. J. Wang, W. Zhang, S. R. Qiu, W. J. Zachowicz, X. Y. Guan, R. Tang, J. R. Hoyer, J. J. De Yoreo and G. H. Nancollas, *J. Cryst. Growth,* **2006**, 291, 160–165.

44 Y. C. Chien, D. L. Masica, J. J. Gray, S. Nguyen, H. Vali and M. D. McKee, *J. Biol. Chem.,* **2009**, 284, 23491−23501.

45 M. Hirose, K. Tozawa, A. Okada, S. Hamamoto, Y. J. Higashibata, B. Gao, Y. Hayashi, H. Shimizu, Y. Kubota, T. Yasui and K. Kohri, *Urol Res,* **2012**, 40, 121–129.

46 Y. Liu and R. Guo, *Biomacromolecules*, **2007**, 8, 2902–2908.

47 Z. Li, A. Shkilnyy and A. Taubert, *Cryst. Growth Des.*, **2008**, 8, 4526–4532

48 Y. Zhang, M. Yang, G. Zhang and D. D. Dionysioub, *Applied Catalysis B: Environmental,* **2013,** 142, 249–258.

49 B. Tomazic and G. H. Nancollas, *Journal of Crystal Growth*, **1979**, 46, 355-361.

50 S. H. Yu, H. Cölfem and M. Antonietti, *J. Phys. Chem. B*, **2003**, 107, 7396–7405.

51 J. Tang and A. P. Alivisatos, *Nano letters*, **2006**, 6, 2701−2706.

52 A. N. Kulak, P. Iddon, Y. T. Li, S. P. Armes, H. Cölfen, O. Paris, R. M. Wilson and F. C. Meldrum, *J. Am. Chem. Soc.*, **2007**, 129, 3729-3736.

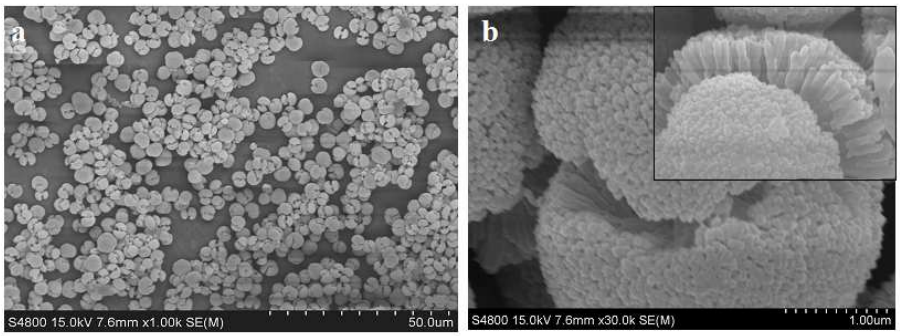


Fig. 1. (a) SEM image of CaOx obtained in the presence of 4.0 g $L^{-1}$ casein at 25 ± 1 °C, [$CaCl_2$ ] = 1.0 mM, showing nearly closed dumbbell-shaped particles; (b) high magnification image of an individual particle.

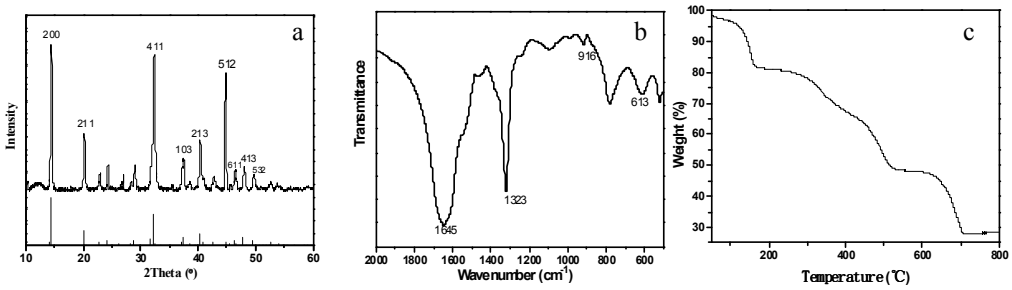


Fig. 2. (a) XRD pattern of nearly closed dumbbell-shaped CaOx (up) and a standard XRD pattern of calcium oxalate dihydrate characterized by the (200), (211), (411), and (213) peaks (down, JCPDS card No. 17-541). (b) FT-IR spectra of nearly closed dumbbell-shaped CaOx showing characterized peak of calcium oxalate dihydrate at 1645 and 1323 $cm^{-1}$. (c) thermogravimetric of dumbbell-shaped CaOx showing the characterized dehydration process of 19.43% at 180 °C (very close to the theoretical value of 20.56% for calcium oxalate dihydrate).

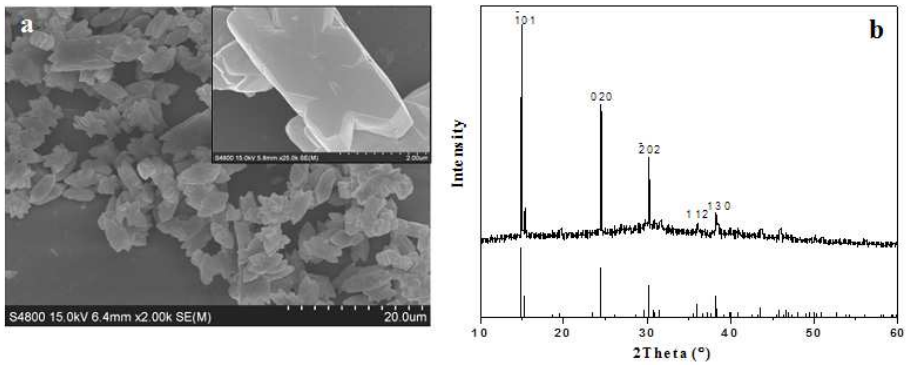


Fig. 3. (a) SEM image of CaOx obtained in the absence of protein at 25 ± 1 °C, [$CaCl_2$ ] = 1.0 mM, showing flowerlike COM agglomerates and hexagonal COM; (b) XRD pattern of the corresponding CaOx (up) and a standard XRD pattern of calcium oxalate monohydrate (down, JCPDS card No. 20-231).

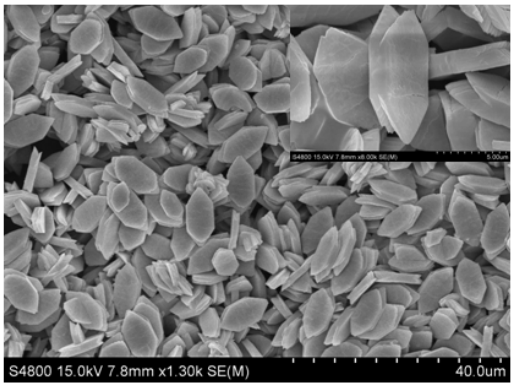


Fig. 4. SEM image of CaOx obtained in the presence of 4.0 g $L^{-1}$ BSA at 25 ± 1 °C, [$CaCl_2$ ] = 1.0 mM, showing elongated hexagonal shape.

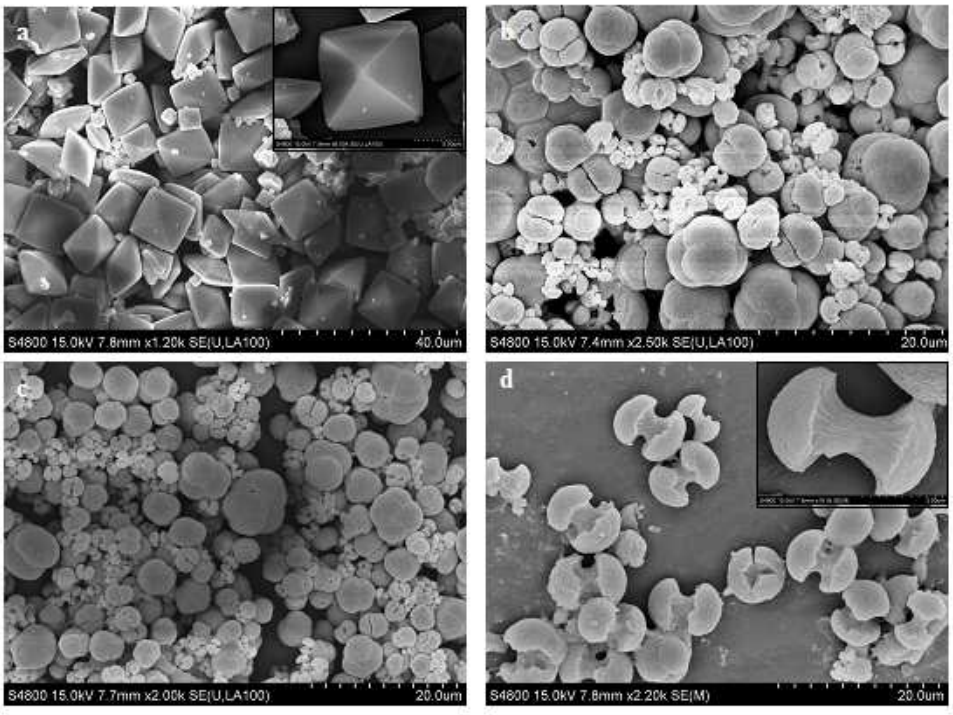


Fig. 5. SEM images of CaOx samples obtained in the presence of casein with different concentrations, [$CaCl_2$ ] = 1.0 mM. [casein] = 0.2 g $L^{-1}$, showing bipyramidal shaped crystal (a); 0.5 g $L^{-1}$, showing nearly closed dumbbell-shaped and twined spherical particles (b); 1 g $L^{-1}$, showing nearly closed dumbbell-shaped and twined spherical particles (c); 6 g $L^{-1}$, showing dumbbell shaped crystal (d).

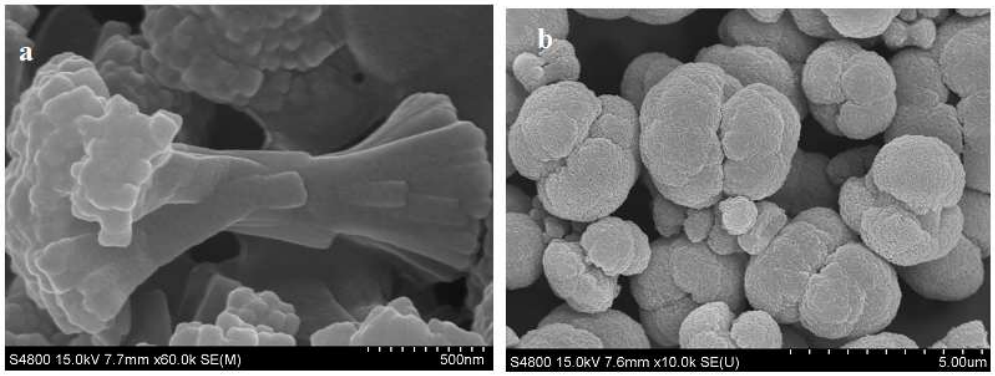


Fig. 6. SEM images of CaOx samples obtained in the presence of 4.0 g $L^{-1}$ casein at 25 °C with different $CaCl_2$ concentrations. (a) [$CaCl_2$] = 0.8 mM, showing dumbbell-shaped crystal; (b) [$CaCl_2$] = 2.0 mM, showing twined spherical particles.

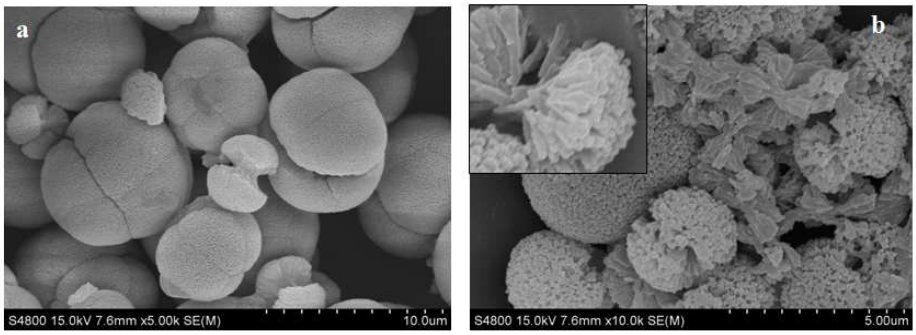


Fig. 7. SEM images of CaOx samples obtained in the presence of 4.0 g $L^{-1}$ casein at (a) 10 °C, showing twined spherical particles and at (b) 37 °C, showing dumbbell shaped crystal with loose structure, [$CaCl_2$ ] = 1.0 mM.

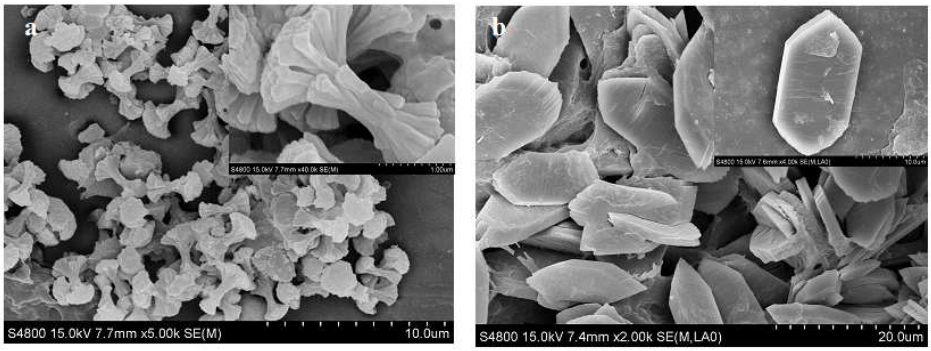


Fig. 8. SEM images of CaOx samples obtained in the presence of 4.0 g $L^{-1}$ casein at (a) pH 10.5, showing dumbbell shaped crystals and (b) pH 3.5, showing elongated hexagonal flake crystals, [$Ca^{2+}$] =1.0 mM.

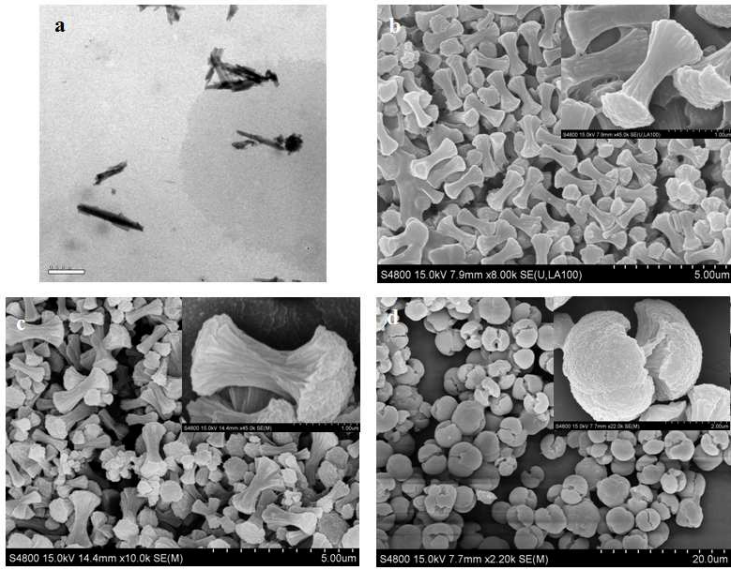


Fig. 9. TEM and SEM images of CaOx samples produced in the presence of 4.0 g $L^{-1}$ casein at the early reaction stages, [$Ca^{2+}$]= 1.0 mM. The reaction time is (a) 30 min, showing nanorods shaped crystals, (b) 3 h, showing nanorod bundle-shaped crystals, (c) 8 h, dumbbell-like nanorod bundles and (d) 12 h, nearly closed dumbbell shaped crystals.

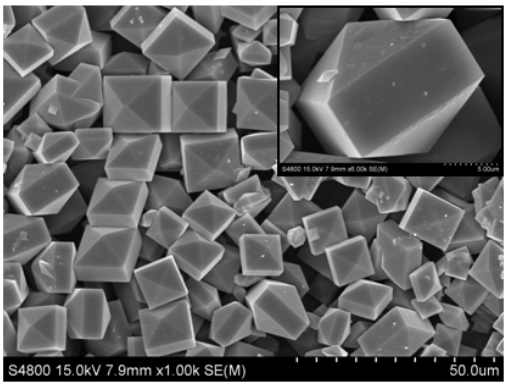


Fig. 10. SEM image of CaOx samples obtained in the presence of 2.0 g $L^{-1}$ casein hydrolysate at 25 ± 1 °C, showing elongated bipyramidal shaped crystals, [$CaCl_2$ ] = 1.0 mM.

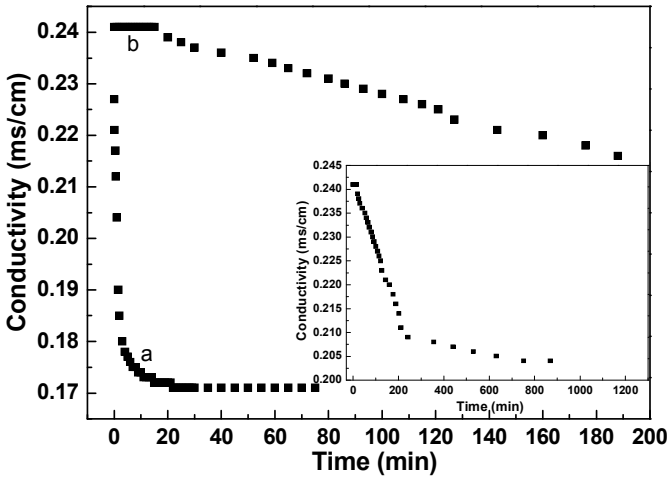


Fig. 11. Conductivity change with time in the growth of CaOx in the $CaCl_2$ and $NaC_2O_4$ aqueous system without (a) and with (b and the inset) casein.

Table 1. $D_{hkl}$ Values Calculated for the (200), (211) and (411) Reflections of Nearly Closed Dumbbell-shaped Crystals.

| *hkl* | 200 | 211 | 411 |
|---|---|---|---|
| $D_{hkl}$ (nm) | 36.2 ± 0.8 | 29.3 ± 0.6 | 27.5 ± 0.5 |

Table 2. Summary of Crystallographic and Morphological Changes of CaOx at Different Reaction Conditions.

| [Casein] (g $L^{-1}$) | $[Ca^{2+}]=[C_2O_4^{2-}]$ (mM) | Temperature (°C) | Starting pH | Phase | Morphology (size) |
|---|---|---|---|---|---|
| 0 | 1.0 | 25 | 6.9 | COM | Agglomerated particles |
| 0.2 | 1.0 | 25 | 6.9 | COD | Bipyramid tetragonal prisms (about 10.2 μm × 9.6 μm) |
| 0.5 | 1.0 | 25 | 6.9 | COD | Nearly closed dumbbell-shaped ( about 4.2 μm) and twined spherical particles (about 8 μm) |
| 1.0 | 1.0 | 25 | 6.9 | COD | Nearly closed dumbbell-shaped (about 4.5 μm) and twined spherical particles (about 6 μm) |
| 4.0 | 1.0 | 25 | 6.9 | COD | Nearly closed dumbbell-shaped particles(about 4.5 μm) |
| 6.0 | 1.0 | 25 | 6.9 | COD | Dumbbell shaped particles (about 10.0 μm × 3.0 μm) |
| 4.0 | 0.8 | 25 | 6.9 | COD | Dumbbell-shaped particles (about 2.0 μm × 0.4 μm) |
| 4.0 | 2.0 | 25 | 6.9 | COD | Twined spherical particles (about 4.0 μm) |
| 4.0 | 1.0 | 10 | 6.9 | COD | Twined spherical particles (about 7.0 μm) |
| 4.0 | 1.0 | 37 | 6.9 | COD | Dumbbell shaped crystal with loose structure |
| 4.0 | 1.0 | 25 | 10.5 | COD | Dumbbell shaped particles (about 3.3 μm × 0.5 μm) |
| 4.0 | 1.0 | 25 | 3.5 | COM | Elongated hexagonal flake |
| 0 | 1.0 | 25 | 10.5 | COT+COM | Tabular and hexagonal crystals |
| 0 | 1.0 | 25 | 3.5 | COM | Flowerlike agglomerates and hexagonal flake |

Table 3. Summary of Inhibition Results of CaOx at Different Reaction Conditions.

| [Casein] (g $L^{-1}$) | $[Ca^{2+}]=[C_2O_4^{2-}]$ (mM) | Temperature (°C) | Starting pH | $k_0/k_i$ | Induction time |
|---|---|---|---|---|---|
| 0 | 1.0 | 25 | 6.9 | 1 | 0 sec |
| 0.2 | 1.0 | 25 | 6.9 | 21.2 | 4 min |
| 0.5 | 1.0 | 25 | 6.9 | 22.7 | 8 min |
| 1.0 | 1.0 | 25 | 6.9 | 43.9 | 10 min |
| 4.0 | 1.0 | 25 | 6.9 | 170.7 | 15 min |
| 6.0 | 1.0 | 25 | 6.9 | 352.0 | 25 min |
| 4.0 | 0.8 | 25 | 6.9 | 232.3 | 20 min |
| 4.0 | 2.0 | 25 | 6.9 | 3.7 | 2 min |
| 4.0 | 1.0 | 10 | 6.9 | 10.3 | 6 sec |
| 4.0 | 1.0 | 37 | 6.9 | 352.0 | 45 min |
| 4.0 | 1.0 | 25 | 10.5 | 68.3 | 4 min |
| 4.0 | 1.0 | 25 | 3.5 | 1.5 | 0 sec |